On the Degrees of Freedom Region for Simultaneous Imaging & Uplink Communication

Nishant Mehrotra, *Student Member, IEEE*, and Ashutosh Sabharwal, *Fellow, IEEE*

***Abstract*—In this paper, we take the first step towards quantifying the fundamental performance trade-offs between imaging and communication supported simultaneously using the same network resources. We analyze an uplink system configuration with a full-duplex base station (BS) illuminating an imaging scene while receiving data from a communication user. Our main contributions are two-fold. First, we propose a unified signal space analysis framework based on the degrees of freedom metric to characterize the trade-offs between the two operations in the high signal-to-noise ratio regime. Second, we propose a dual-function joint processing scheme, decode-and-image, that allows the BS to simultaneously form an image of the scene while decoding the uplink user's data. Our analysis and proposed scheme highlight the benefits of exploiting the uplink signals for imaging, at the cost of increased cooperation between the BS and uplink user. Moreover, our proposed scheme outperforms traditional schemes that enable dual-function operation via spatial or temporal isolation of imaging and communication signals.**

***Index Terms*—Degrees of freedom, joint imaging and communication, multiple-input multiple-output, wireless imaging.**

I. Introduction

THE next generation of wireless networks are expected to deploy massive multiple-input multiple-output (MIMO) base stations with hundreds to thousands of antennas and operate at higher frequencies in the millimeter-wave band compared to current sub-6 GHz systems. The larger bandwidths in millimeter-wave bands and fine-grained beamsteering capabilities of massive MIMO arrays open up novel possibilities for performing *sensing*, such as radar, orientation estimation and imaging, simultaneously alongside traditional communication.

In this paper, we focus on the special case of performing *imaging* alongside traditional data communication, a scenario we term simultaneous imaging and communication. By imaging, we refer to the operation of forming a spatial estimate of the material properties of the surrounding environment. While the idea of imaging using wireless signals is not new, e.g., see prior work on Wi-Fi [2]–[5], millimeter-wave [6]–[9] and radar imaging [10]–[13], the majority of prior work is representative of *imaging-only* operation where the communication data is known a-priori. To the best of our knowledge, performing both imaging and communication decoding with the same network resources is a key challenge that has remained open thus far.

Manuscript received July 30, 2021; revised December 9, 2021; accepted January 14, 2022. This work was partially supported by the NSF under grant CNS-1956297. The material in this paper was presented in part at the 2021 55th Asilomar Conference on Signals, Systems, and Computers [1].

The authors are with the Department of Electrical and Computer Engineering, Rice University, Houston, TX, 77005, USA. E-mail: {nm30, ashu}@rice.edu.

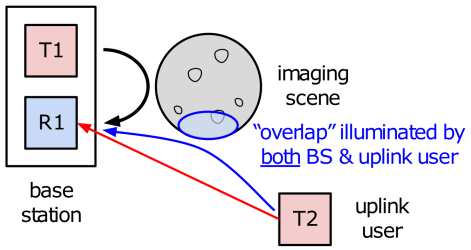

Fig. 1: Simultaneous imaging & uplink communication.

To that end, in this paper we take the first step towards quantifying the fundamental performance trade-offs between imaging and communication supported simultaneously using the same network resources. We analyze the *uplink* system configuration shown in Figure 1, with a full-duplex base station (BS) actively illuminating a subset of the environment (labeled imaging scene) while receiving uplink signals transmitted by a communication user. The system analyzed is the dual-function equivalent of the multiple access channel [14], in that the BS aims to image the scene and decode the uplink user's data from a common set of received measurements.

Our contributions in this paper are two-fold. First, we adapt the well-known *signal space* framework [15]–[19] to characterize the performance trade-offs between imaging and communication under a space-time-frequency constraint on the resources available to the BS. To bridge the dichotomy between the performance metrics used for imaging- and communication-only operations, namely the imaging resolution and communication rate, we propose using the *degrees of freedom* (DoF) as a unified dual-function metric. With every simultaneous imaging and communication scheme, we associate a DoF pair $(d_{\mathsf{img}}, d_{\mathsf{comm}})$ if (i) the maximum number of distinct point scatterers in the scene that can be spatially differentiated in the image reconstruction equals d_{img}, and (ii) the achievable rate scales as $d_{\mathsf{comm}} \cdot \log_2(\mathsf{SNR})$. We characterize the performance trade-offs between imaging and communication by deriving the *DoF region*, the set of all DoF pairs $(d_{\mathsf{img}}, d_{\mathsf{comm}})$ that are simultaneously achievable, under a fixed space-time-frequency constraint on the BS resources.

Second, we propose a dual-function joint processing scheme, *decode-and-image*, that allows the BS to simultaneously form an image of the scene while decoding the uplink user's data. As the name suggests, the BS first decodes the uplink user's data, which is subsequently used as side-information for imaging. Decode-and-image has better dual-function performance compared to traditional schemes that enable dual-function operation via spatial or temporal isolation of imaging and communication signals, e.g., time-sharing.

The system-level implications of our DoF analysis are as follows. Consider the general scenario shown in Figure 1, where a portion of the scene (labeled overlap) is illuminated by *both* the BS and the uplink user. For this general scenario, our DoF analysis predicts an imaging resolution benefit to the additional uplink illumination, since the BS-uplink user pair effectively serves as a hybrid monostatic-multistatic illumination source. However, the better imaging performance comes at the cost of requiring the BS and uplink user to *cooperate* by means of sending known pilot sequences. As we show in our DoF analysis, the required cooperation results in a smaller achievable communication decoding rate compared to the maximum possible. In our results, we derive the optimal number of uplink pilots required in the proposed decode-and-image scheme for the BS to decode and exploit the uplink data as additional imaging illumination.

Although decode-and-image is not optimal in general, we show that it is asymptotically optimal, i.e., the gap between the achievable DoF region with decode-and-image and the dual-function DoF region is vanishingly small under the limit of large channel coherence intervals. Moreover, in the special case where the scene is only illuminated by the uplink signals, decode-and-image enables *opportunistic* imaging for a small reduction in the achievable uplink rate.

A. Comparison with Prior Work

To the best of our knowledge, we are the first to study the simultaneous imaging and communication problem. Related work includes joint sensing-communication [20]–[22] and joint radar-communication [23]–[28].

The former papers [20]–[22] characterize the trade-offs between the sensing estimation error and communication rate via rate-distortion theory. However, the estimation error is not an interpretable performance metric for imaging, for which a more meaningful metric is the *resolution* - the minimum distance at which two distinct point scatterers can be spatially differentiated in the image reconstruction. While resolution limits for imaging-only systems (where the communication data is known a-priori) are well-understood via the main results of [29]–[32], the trade-offs between the achievable imaging resolution and communication rate in dual-function systems have not been characterized previously.

The latter papers [23]–[28] are concerned with the design of joint radar-communication systems. For a system model similar to ours, it is shown in [23], [24], [26]–[28] that exploiting the communication signals bouncing off the scene is beneficial for radar detection. However, the underlying requirements in [23], [24], [26]–[28] are (i) known second-order statistics of the uplink symbols at the BS, and (ii) uncorrelated measurements at the BS, both of which may be invalid in practice. Our analysis removes both requirements by using a signal space model for Figure 1 that explicitly takes into account spatial correlation between antennas and does not require any prior knowledge of the uplink symbols at the BS. Moreover, the cost of decoding the uplink signals is not quantified in [23], [24], [26]–[28]. As we show in our main results, the better imaging performance due to additional uplink illumination comes at the cost of a smaller uplink rate.

Finally, the authors in [25] analyze a special case of Figure 1 with no uplink signals bouncing off the imaging scene. In this case, a zero-forcing-based successive interference cancellation scheme is proposed in [25], along with associated inner bounds on the dual-function performance. However, the optimality of zero-forcing is not discussed in [25]. In Section V-A, we show that in this regime (i) the proposed decode-and-image scheme reduces to zero-forcing, and (ii) the inner bound for decode-and-image matches the outer bound on the dual-function DoF region, i.e., both zero-forcing and decode-and-image are optimal. Moreover, for the general setting shown in Figure 1, we show that zero-forcing is strictly sub-optimal and achieves a subset of the inner bound with decode-and-image.

The remainder of this paper is organized as follows. In Section II, we present the system model for Figure 1. We define the degrees of freedom performance metric and formulate the main problem we solve in this paper in Section III. We present our theoretical results in Section IV, and provide a system-level illustration for them in Section V. We conclude the paper in Section VI with discussions and directions for future work.

B. Notation

We use bold uppercase for matrices (e.g., $\mathbf{X}$), bold lowercase for vectors (e.g., $\mathbf{x}$) and non-bold lowercase for scalars (e.g., x). Sets are represented using calligraphic font (e.g., $\mathcal{X}$) or capital Greek letters (e.g., Ω). The $n \times n$ identity matrix and nth standard basis vector are $\mathbf{I}_n$ and $\mathbf{e}_n$ respectively. The matrix, Kronecker and column-wise Khatri-Rao products are denoted by $\cdot$, $\otimes$ and $*$ respectively. The transpose, Hermitian and pseudo-inverse operators are $(\cdot)^\top$, $(\cdot)^H$ and $(\cdot)^\dagger$ respectively. Vectorization and diagonalization are denoted by $\mathsf{vec}(\cdot)$ and $\mathsf{diag}(\cdot)$. The positive part of a scalar x is $[x]^+$. The set union, intersection, and difference operators are $\cup$, $\cap$, and $\setminus$. The Lebesgue measure of a set $\mathcal{X}$ is denoted by $|\mathcal{X}|$.

II. System Model

Consider the system shown in Figure 1, with a full duplex base station (BS) illuminating a subset of the environment, labeled *imaging scene*, while receiving data from a communication user. Without loss of generality, we make the following assumptions on the system operation.

Assumption 1: The scatterers in the environment remain static for T slots, which determines the coherence interval.

Assumption 2: The BS and uplink user signalling is unipolarized, with operating wavelength λ.

Assumption 3: There is perfect self-interference cancellation between the BS transmitter and receiver.

We note that Assumption 2 is made only for analytical simplicity. Extensions of our results to the generic arbitrarily polarized, broadband setting are straightforward via the results of [16], [32], and are omitted due to space constraints.

Given Assumptions 1-3 hold, the receive measurements at the BS correspond to the sum of the uplink user transmissions and the backscatter from the scene. Without loss of generality, we assume the imaging scene is discretized into M *voxels*, spaced at distances much smaller than the Rayleigh resolution limit of $\frac{\lambda}{2}$ [19], [30], [31]. Furthermore, let $K_{TX}^{(i)}$, $K_{TX}^{(c)}$

and K_{RX} respectively denote the number of antennas at the BS transmitter, uplink user and BS receiver. Within a coherence interval of T slots, the $K_{RX} \times T$ matrix of receive measurements, $\mathbf{Y}_T$, is given by

$$\mathbf{Y}_T = \mathbf{H}^{(c)} \cdot \mathbf{X}_T^{(c)} + \mathbf{P}_{RX}^{(i)} \cdot \mathsf{diag}\left(\mathbf{f}\right) \cdot \left(\mathbf{P}_{TX}^{(i)}\right)^{\top} \cdot \mathbf{X}_T^{(i)} + \mathbf{N}_T. \quad (1)$$

The first term in (1) corresponds to the received uplink symbols. The matrix $\mathbf{X}_T^{(c)}$ in (1) is the $K_{TX}^{(c)} \times T$ matrix of transmitted uplink symbols, while $\mathbf{H}^{(c)}$ is the $K_{RX} \times K_{TX}^{(c)}$-sized uplink channel matrix.

The second term in (1) corresponds to the backscatter from the imaging scene due to BS illumination. In (1), $\mathbf{X}_T^{(i)}$ is the $K_{TX}^{(c)} \times T$ matrix of transmitted BS illumination symbols. Furthermore, the $M \times 1$ *scene reflectivity* vector $\mathbf{f}$ models the material properties of the M voxels in the scene. As the name suggests, the squared magnitude of a voxel's reflectivity is the energy reflected by it upon illumination by a unit energy field. Such a reflectivity-based formulation is extremely generic since a zero or non-zero reflectivity respectively indicates the absence or presence of a scatterer at a given scene voxel.

The $K_{TX}^{(i)} \times M$ and $K_{RX} \times M$-sized *path delay matrices* $\mathbf{P}_{TX}^{(i)}$ and $\mathbf{P}_{RX}^{(i)}$ model signal propagation to and from the scene. The (k,m)th element of each path delay matrix is a scaled complex exponential that depends on the signalling wavelength λ, and the locations of the kth antenna at the BS and mth voxel in the scene [15]–[17], [19],

$$\mathbf{P}_{TX/RX}^{(i)}(k,m) = \frac{e^{-j\left(\frac{2\pi}{\lambda}\right)\left\|\mathbf{r}_k^{TX/RX} - \tilde{\mathbf{r}}_m\right\|_2}}{4\pi \cdot \left\|\mathbf{r}_k^{TX/RX} - \tilde{\mathbf{r}}_m\right\|_2}, \quad (2)$$

where $\mathbf{r}$ and $\tilde{\mathbf{r}}$, with appropriate subscripts and superscripts, denote the position vectors of the antennas and scene voxels.

Finally, $\mathbf{N}_T$ is the $K_{RX} \times T$ matrix of additive noise in (1). In the next section, we formulate the simultaneous imaging and communication problem we solve in this paper.

III. Problem Formulation

In the system in Figure 1, the BS aims to perform the following two functions using the received measurements $\mathbf{Y}_T$:

1) **Imaging:** Form a spatial estimate of the material properties of scatterers present in the imaging scene, i.e., estimate the scene reflectivity vector $\mathbf{f}$, and
2) **Communication:** Decode the uplink user's data, i.e., estimate the uplink symbol matrix $\mathbf{X}_T^{(c)}$.

Our goal in this paper is to understand the fundamental performance trade-offs between the two functions supported simultaneously using the same network resources at the BS. Specifically, we answer the following question:

> Given a *constraint* in space-time-frequency on the available resources, what combinations of the imaging resolution and uplink communication rates can the BS reliably support? (Q)

We answer (Q) via a signal space analysis [15]–[19], with the degrees of freedom (DoF) as the dual-function metric of choice. At a high-level, the DoF captures the high-SNR scaling behavior of the achievable communication rate and the maximum number of distinct point scatterers in the scene that can be spatially differentiated in the image reconstruction. We first define the DoF metric in Section III-A. We then formulate (Q) in terms of the DoF framework in Section III-B.

A. Performance Metric: Degrees of Freedom

We begin by defining the imaging DoF. To that end, we first define the notion of *linear imaging algorithms* as follows.

Definition 1: A linear imaging algorithm takes as input a measurement vector $\mathbf{y}$ and a side-information set $\mathcal{S}$, and outputs a reconstruction $\hat{\mathbf{f}}$ of the true $M \times 1$ reflectivity vector $\mathbf{f}$ that is expressible as a linear function of $\mathbf{f}$,

$$\hat{\mathbf{f}} = \mathbf{A}^{(\mathbf{y},\mathcal{S})} \cdot \mathbf{f} + \mathbf{w},$$

where $\mathbf{w}$ is an $M \times 1$ additive noise vector and $\mathbf{A}^{(\mathbf{y},\mathcal{S})}$ is an $M \times M$ square mapping from the scene to itself.

Let us consider a simple example to illustrate Definition 1.

Example 1: Consider the system model in (1) in the special case with known uplink symbols $\mathbf{X}_T^{(c)}$ (e.g., pilots), channel matrix $\mathbf{H}^{(c)}$, and path delay matrices $\left\{\mathbf{P}_{TX}^{(i)}, \mathbf{P}_{RX}^{(i)}\right\}$. In this case, we have $\mathcal{S} = \left\{\mathbf{X}_T^{(c)}, \mathbf{H}^{(c)}, \mathbf{P}_{TX/RX}^{(i)}\right\}$ and $\mathbf{y} = \mathsf{vec}\left(\mathbf{Y}_T\right)$. An example of a linear imaging algorithm corresponds to subtracting out the communication signals $\mathbf{H}^{(c)} \cdot \mathbf{X}_T^{(c)}$ from $\mathbf{Y}_T$ and recovering $\mathbf{f}$ appropriately,

$$\begin{aligned}\hat{\mathbf{f}} &= \left(\mathbf{H}_{\mathsf{vec}}^{(i)}\right)^{\dagger} \cdot \mathsf{vec}\left(\mathbf{Y}_T - \mathbf{H}^{(c)} \cdot \mathbf{X}_T^{(c)}\right) \\ &= \left(\mathbf{H}_{\mathsf{vec}}^{(i)}\right)^{\dagger} \cdot \mathbf{H}_{\mathsf{vec}}^{(i)} \cdot \mathbf{f} + \left(\mathbf{H}_{\mathsf{vec}}^{(i)}\right)^{\dagger} \cdot \mathbf{n}_T,\end{aligned}$$

where $\mathbf{n}_T = \mathsf{vec}\left(\mathbf{N}_T\right)$ is the vectorized version of $\mathbf{N}_T$, and

$$\mathbf{H}_{\mathsf{vec}}^{(i)} = \left(\left(\mathbf{X}_T^{(i)}\right)^{\top} \otimes \mathbf{I}_{K_{RX}}\right) \cdot \left(\mathbf{P}_{TX}^{(i)} * \mathbf{P}_{RX}^{(i)}\right),$$

for Kronecker and column-wise Khatri-Rao products $\otimes$ and $*$, and $\mathbf{I}_n$ denoting the identity matrix of size $n \times n$.

Note that the reconstruction $\hat{\mathbf{f}}$ above is linear in $\mathbf{f}$. Since we do not impose any additional assumptions on the scene besides Assumption 1, the linearity of the system model in (1) in $\mathbf{f}$ makes it sufficient to consider only linear imaging algorithms in this paper. We note that this *does not* limit the generality of our results since even with additional sparsity assumptions on the scene, the minimum separation required between scatterers for compressive sensing-based imaging is similar to traditional Rayleigh resolution limits for linear imaging algorithms [11]. Hence, it suffices to quantify the imaging performance for linear imaging algorithms in the sequel.

To that end, we use the number of *resolvable voxels*, i.e., the number of distinct point scatterers in the scene that can be spatially differentiated in the image reconstruction [16], [19], as our performance metric. Formally, we quantify the same via the *dimensionality* of the space of scene reconstructions $\hat{\mathbf{f}}$.

The dimensionality of a set is defined as follows.

Definition 2 ([19], [33]): Consider a subset $\mathcal{A}$ of a normed linear space $\mathcal{X}$ of unit norm signals. The dimensionality of $\mathcal{A}$ is the dimension of the minimal subspace that can approximate the elements of $\mathcal{A}$ up to arbitrarily small accuracy, i.e.,

$$\mathsf{dim}\left(\mathcal{A}\right) = \min\left\{n : \rho_n\left(\mathcal{A}\right) = 0\right\},$$

where $\rho_n(\mathcal{A})$ is the smallest distance between $\mathcal{A}$ and all possible n-dimensional subspaces $\mathcal{X}_n$ of $\mathcal{X}$,

$$\rho_n(\mathcal{A}) = \inf_{\mathcal{X}_n \subseteq \mathcal{X}} \sup_{f \in \mathcal{A}} \inf_{g \in \mathcal{X}_n} \|f - g\|.$$

Given Definition 2, we define the imaging DoF as follows.

Definition 3: Let $\mathcal{F}_{(\mathbf{y},\mathcal{S})}$ denote the set of all noiseless unit-normalized outputs $\hat{\mathbf{f}}$ of a linear algorithm with matrix $\mathbf{A}^{(\mathbf{y},\mathcal{S})}$,

$$\mathcal{F}_{(\mathbf{y},\mathcal{S})} = \left\{ \hat{\mathbf{f}} : \hat{\mathbf{f}} = \mathbf{A}^{(\mathbf{y},\mathcal{S})} \cdot \mathbf{f}, \ \left\| \hat{\mathbf{f}} \right\|_2^2 \leq 1 \right\}.$$

The imaging DoF, d_{img}, corresponding to $\mathbf{A}^{(\mathbf{y},\mathcal{S})}$ is defined as the dimensionality of the set $\mathcal{F}_{(\mathbf{y},\mathcal{S})}$,

$$d_{\mathsf{img}} = \mathsf{dim}\left(\mathcal{F}_{(\mathbf{y},\mathcal{S})}\right) = \min\left\{ n : \rho_n\left(\mathcal{F}_{(\mathbf{y},\mathcal{S})}\right) = 0 \right\}.$$

We note that the unit normalization in Definition 3 is only for consistency with Definition 2 and has no effect on the DoF value. Furthermore, since $\mathcal{F}_{(\mathbf{y},\mathcal{S})}$ is a subset of the column space of $\mathbf{A}^{(\mathbf{y},\mathcal{S})}$, Definition 3 is equivalent to [33]

$$\rho_n\left(\mathcal{F}_{(\mathbf{y},\mathcal{S})}\right) = \sigma_{n+1}\left(\mathbf{A}^{(\mathbf{y},\mathcal{S})}\right),$$

where $\sigma_k\left(\mathbf{A}^{(\mathbf{y},\mathcal{S})}\right)$ denotes the kth singular value of $\mathbf{A}^{(\mathbf{y},\mathcal{S})}$. Therefore, the imaging DoF for a linear algorithm is simply the rank of the matrix $\mathbf{A}^{(\mathbf{y},\mathcal{S})}$, i.e., the smallest index n beyond which the singular values of $\mathbf{A}^{(\mathbf{y},\mathcal{S})}$ decay to 0,

$$\begin{aligned} d_{\mathsf{img}} &= \min\left\{ n : \sigma_{n+1}\left(\mathbf{A}^{(\mathbf{y},\mathcal{S})}\right) = 0 \right\} \\ &= \mathsf{rank}\left(\mathbf{A}^{(\mathbf{y},\mathcal{S})}\right). \end{aligned}$$

Note that for a generic linear system model, $\mathbf{y} = \mathbf{H}^{(i)} \cdot \mathbf{f} + \mathbf{n}$, the matrix $\mathbf{A}^{(\mathbf{y},\mathcal{S})}$ may be decomposed as follows,

$$\mathbf{A}^{(\mathbf{y},\mathcal{S})} = \mathbf{B}^{(\mathcal{S})} \cdot \mathbf{H}^{(i)},$$

i.e., in terms of the channel $\mathbf{H}^{(i)}$ and a matrix $\mathbf{B}^{(\mathcal{S})}$ that only depends on the side-information available to the algorithm. For example, $\mathbf{B}^{(\mathcal{S})} = \left(\mathbf{H}^{(i)}_{\mathsf{vec}}\right)^{\dagger}$ and $\mathbf{H}^{(i)} = \mathbf{H}^{(i)}_{\mathsf{vec}}$ for Example 1.

Hence, the imaging DoF is upper bounded as

$$d_{\mathsf{img}} = \min\left\{ \mathsf{rank}\left(\mathbf{B}^{(\mathcal{S})}\right), \mathsf{rank}\left(\mathbf{H}^{(i)}\right) \right\} \leq \mathsf{rank}\left(\mathbf{H}^{(i)}\right). \quad (3)$$

Depending on the conditioning of $\mathbf{H}^{(i)}$, the number of resolvable voxels may thus be smaller than M if $\mathsf{rank}\left(\mathbf{H}^{(i)}\right) \ll M$.

Finally, we note that Definition 3 associates an imaging DoF value to a particular algorithm, and is in a sense analogous to defining the rate of a given coding scheme. Furthering the analogy, we now define the notion of *achievability* for imaging.

Definition 4: An imaging DoF of d_{img} is achievable if there exists a linear imaging algorithm with matrix $\mathbf{A}^{(\mathbf{y},\mathcal{S})}$ such that

$$d_{\mathsf{img}} = \mathsf{rank}\left(\mathbf{A}^{(\mathbf{y},\mathcal{S})}\right).$$

For instance, the DoF upper bound in (3) is achievable by a linear imaging algorithm with $\mathbf{B}^{(\mathcal{S})} = \left(\mathbf{H}^{(i)}\right)^{\dagger}$.

We now consider communication. With standard definitions for achievable rates, mutual information, etc., e.g., see [14, Chapter 7], we define the *communication DoF* as follows.

Definition 5: Let a rate R be achievable. The achievable communication DoF, d_{comm}, is a high-SNR approximation of the achievable rate, scaled by the coherence interval T,

$$d_{\mathsf{comm}} = T \cdot \lim_{\mathsf{SNR}\to\infty} \frac{R}{\frac{1}{2} \cdot \log_2(1 + \mathsf{SNR})}.$$

Barring the scaling factor T, we note that the above definition is identical to the DoF definition commonly used in the wireless literature, e.g., see [16], [18], [34], [35]. However, the conventional definition only corresponds to the *spatial* DoF, a.k.a. spatial multiplexing gain. We scale the conventional definition by T in order to characterize the *space-time* DoF.

For a standard MIMO system model, $\mathbf{Y}_T = \mathbf{H} \cdot \mathbf{X}_T + \mathbf{N}_T$, d_{comm} may be upper bounded as [36, Chapter 7],

$$d_{\mathsf{comm}} \leq T \cdot \mathsf{rank}(\mathbf{H}), \quad (4)$$

i.e., as the product of the coherence interval T and the rank of the channel matrix $\mathbf{H}$. Furthermore, the DoF upper bound is achievable with appropriate beamforming on the basis of $\mathbf{H}$.

B. Problem Formulation: Signal Space DoF Analysis

We are now ready to pose (Q) in terms of the DoF framework. To that end, let us rewrite (1) as a linear equation with the scene reflectivities and uplink symbols as the input,

$$\mathbf{y}_T = \begin{bmatrix} \mathbf{H}^{(i)}_{\mathsf{vec}} & \mathbf{H}^{(c)}_{\mathsf{vec}} \end{bmatrix} \cdot \begin{bmatrix} \mathbf{f} \\ \mathbf{x}^{(c)}_T \end{bmatrix} + \mathbf{n}_T, \quad (5)$$

$$\mathbf{H}^{(i)}_{\mathsf{vec}} = \left(\left(\mathbf{X}^{(i)}_T\right)^{\top} \otimes \mathbf{I}_{K_{RX}} \right) \cdot \left(\mathbf{P}^{(i)}_{TX} * \mathbf{P}^{(i)}_{RX} \right), \quad (6)$$

$$\mathbf{H}^{(c)}_{\mathsf{vec}} = \mathbf{I}_T \otimes \mathbf{H}^{(c)}, \quad (7)$$

where $\otimes$ and $*$ denote the Kronecker and column-wise Khatri-Rao products respectively, and $\mathbf{I}_n$ denotes the identity matrix of size $n \times n$. Answering (Q) requires first characterizing the total resources available at the BS in space-time-frequency.

To that end, recall from (3) and (4) that the imaging and communication DoFs for (5) may be upper bounded as

$$\left\{ d_{\mathsf{img}} \leq \mathsf{rank}\left(\mathbf{H}^{(i)}_{\mathsf{vec}}\right), \ d_{\mathsf{comm}} \leq \mathsf{rank}\left(\mathbf{H}^{(c)}_{\mathsf{vec}}\right) \right\}.$$

The rank interpretation of both DoF definitions above naturally prompts defining the total BS resource as the rank of the combined channel $\begin{bmatrix} \mathbf{H}^{(i)}_{\mathsf{vec}} & \mathbf{H}^{(c)}_{\mathsf{vec}} \end{bmatrix}$ in (5).

Definition 6: For the system model in (5), the total resource in space-time-frequency available to the BS receiver is

$$d_{\mathsf{BS}} = \mathsf{rank}\left(\begin{bmatrix} \mathbf{H}^{(i)}_{\mathsf{vec}} & \mathbf{H}^{(c)}_{\mathsf{vec}} \end{bmatrix} \right).$$

Given the above definition, we answer (Q) by deriving the dual-function *DoF region*.

Definition 7: The DoF region, $\mathcal{D}$, is the convex closure of all DoF pairs, $(d_{\mathsf{img}}, d_{\mathsf{comm}})$, that are simultaneously achievable with d_{BS} total space-time-frequency BS resource, where achievability and d_{BS} are as defined in Definitions 4, 5 and 6.

To obtain physically interpretable results, we use a *signal space* framework [15]–[19] to derive the DoF region for our system. In the signal space framework, the BS resources are characterized in terms of (i) the spatial size of the aperture, (ii) the spatial geometry of scatterers in the environment, and

(iii) the coherence interval T. The signal space framework directly takes into account practical wireless effects, such as correlated fading across antennas [15]–[19], and removes limiting assumptions made in prior work [23], [24], [26]–[28] on the spatially uncorrelated nature of BS measurements $\mathbf{Y}_T$.

The signal space representation of Figure 1 is shown in Figure 2. As shown, we equip the BS and uplink user with continuous apertures, modeled as spheres of radii b_{TX}, b_{RX} and c_{TX}. Furthermore, we characterize the spatial geometry of scatterers in the environment in the angular domain, with $\Omega_{TX}^{(i)}$ and $\Omega_{RX}^{(i)}$ denoting the set of angles over which the BS illuminates the imaging scene and receives the backscattered signals. Similarly, $\Omega_{TX}^{(c)}$ and $\Omega_{RX}^{(c)}$ denote the set of angles over which the uplink signals emanate from the uplink user and impinge onto the BS receiver. Note that all angular intervals are shown to be angularly contiguous purely for the sake of illustration in Figure 2. Via the main results of [15]–[18], all our subsequent results hold as-is even when $\Omega_{TX}^{(c)}$, $\Omega_{RX}^{(c)}$, $\Omega_{TX}^{(i)}$ and $\Omega_{RX}^{(i)}$ are the union of multiple smaller angular intervals.

For the signal space model in Figure 2, the total BS resource d_{BS} corresponds to the product of the coherence interval T, the wavelength-normalized aperture size, and the total angular interval over which the imaging and communication signals impinge onto the BS receiver [15]–[19],

$$d_{\mathsf{BS}} = \frac{2T}{\lambda} \cdot b_{RX} \cdot \left| \Omega_{RX}^{(i)} \cup \Omega_{RX}^{(c)} \right|. \tag{8}$$

Moreover, the signal space framework places a deterministic limit on the ranks of the channel and path delay matrices in (1).

Lemma 1 ([15]–[19]): For the system model in (1),

$$\lim_{\substack{K_{TX}^{(c)} \to \infty \\ K_{RX} \to \infty}} \mathsf{rank}\left(\mathbf{H}^{(c)}\right) = \tfrac{2}{\lambda} \cdot \min\left\{ c_{TX} \cdot \left|\Omega_{TX}^{(c)}\right|, b_{RX} \cdot \left|\Omega_{RX}^{(c)}\right| \right\},$$

$$\lim_{\substack{K \to \infty \\ M \to \infty}} \mathsf{rank}\left(\mathbf{P}\right) = \frac{2a}{\lambda} \cdot \left|\Omega\right|,$$

where for $\mathbf{P} \in \left\{ \mathbf{P}_{TX}^{(i)}, \mathbf{P}_{RX}^{(i)} \right\}$, we have $K \in \left\{ K_{TX}^{(i)}, K_{RX} \right\}$, $a \in \{b_{TX}, b_{RX}\}$ and $\Omega \in \left\{ \Omega_{TX}^{(i)}, \Omega_{RX}^{(i)} \right\}$ respectively.

In the following section, we present main results characterizing the DoF region $\mathcal{D}$ for the signal space model in Figure 2.

IV. Main Results

We follow the conventional converse-achievability information theoretic approach to characterize the DoF region $\mathcal{D}$. In Section IV-A, we derive an outer bound $\mathcal{D}_{\mathsf{out}}$ such that $\mathcal{D} \subseteq \mathcal{D}_{\mathsf{out}}$, that holds regardless of the post-processing performed at the BS. We then present a new scheme called *decode-and-image* in Section IV-B, and derive a corresponding an achievable inner bound such that $\mathcal{D}_{\mathsf{in}} \subseteq \mathcal{D}$, in Section IV-C. We characterize the gap between the inner and outer bounds in Section IV-D. We provide a system-level illustration of our results later in Section V.

All our results are derived under the following assumptions.

Assumption 4: Consider the uplink channel matrix $\mathbf{H}^{(c)}$ in (1). Given a non-empty overlap between the receive imaging and communication angular intervals, $\Omega_{RX}^{(i)} \cap \Omega_{RX}^{(c)} \neq \emptyset$, $\mathbf{H}^{(c)}$ may be decomposed into the sum of an a-priori known channel matrix $\mathbf{H}_{\mathsf{known}}^{(c)}$ and an a-priori unknown matrix corresponding to backscatter from the scene due to uplink user illumination,

$$\mathbf{H}^{(c)} = \mathbf{H}_{\mathsf{known}}^{(c)} + \mathbf{P}_{RX}^{(c\cap i)} \cdot \mathsf{diag}\left(\mathbf{f}\right) \cdot \left(\mathbf{P}_{TX}^{(c\cap i)}\right)^{\top} \cdot \mathbf{X}_T^{(c)}.$$

In the equation above, $\mathbf{P}_{TX}^{(c\cap i)}$ and $\mathbf{P}_{RX}^{(c\cap i)}$ are path delay matrices corresponding to signal propagation from the uplink user to the scene and the overlapping angular interval $\Omega_{RX}^{(i)} \cap \Omega_{RX}^{(c)}$ to the BS. Equivalently, Lemma 1 holds for $\mathbf{P} \in \left\{ \mathbf{P}_{TX}^{(c\cap i)}, \mathbf{P}_{RX}^{(c\cap i)} \right\}$ with $K \in \left\{ K_{TX}^{(c)}, K_{RX} \right\}$, $a \in \{c_{TX}, b_{RX}\}$ and $\Omega \in \left\{ \Omega_{TX}^{(c\cap i)}, \Omega_{RX}^{(i)} \cap \Omega_{RX}^{(c)} \right\}$, where $\Omega_{TX}^{(c\cap i)} \subseteq \Omega_{TX}^{(c)}$ corresponds to the uplink user-illuminated portion of scene.

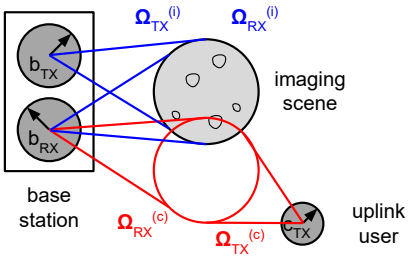

Fig. 2: Signal space representation of Figure 1 with continuous apertures at all nodes and angular domain modeling of the environment. Variables corresponding to BS illumination and uplink user transmission are in blue and red color respectively.

Assumption 5: All path delay matrices $\mathbf{P}_{TX}^{(i)}$, $\mathbf{P}_{RX}^{(i)}$, $\mathbf{P}_{TX}^{(c\cap i)}$ and $\mathbf{P}_{RX}^{(c\cap i)}$ are known to the BS and uplink user.

Assumptions 4 and 5 are simplifying assumptions that are the dual-function equivalents of having channel state information at all nodes in a multiple access channel. Hence, our resulting DoF bounds quantify the *best achievable* dual-function performance. We note that knowledge of path delay matrices may be obtained via an *imaging calibration* phase prior to the system operation. Examples include scanning a point target with known reflectivity across every voxel in the imaging scene [37] or the uplink user sharing the location coordinates of its aperture with the BS. Extensions to scenarios with no such prior knowledge are left for future work.

We are now ready to present our main results, beginning with an outer bound on the DoF region.

A. Outer Bound $\mathcal{D}_{\mathsf{out}}$ on DoF Region

The following theorem characterizes the outer bound $\mathcal{D}_{\mathsf{out}}$.

Theorem 1: An outer bound $\mathcal{D}_{\mathsf{out}}$ on the DoF region $\mathcal{D}$ is the convex closure of all DoF pairs $(d_{\mathsf{img}}, d_{\mathsf{comm}})$ that satisfy

$$d_{\mathsf{img}} \leq \frac{2}{\lambda} \cdot \min\Big\{ b_{RX} \cdot \left|\Omega_{RX}^{(i)}\right| \cdot \chi, b_{TX} \cdot \left|\Omega_{TX}^{(i)}\right| + c_{TX} \cdot \left|\Omega_{TX}^{(c\cap i)}\right| + b_{RX} \cdot \left|\Omega_{RX}^{(i)}\right| \Big\},$$

$$\chi = \lim_{\substack{K_{TX}^{(i)} \to \infty \\ K_{TX}^{(c)} \to \infty}} \mathsf{rank}\left(\begin{bmatrix} \mathbf{X}_T^{(i)} \\ \mathbf{X}_T^{(c)} \end{bmatrix} \right),$$

$$d_{\mathsf{comm}} \leq \frac{2T}{\lambda} \cdot \min\left\{ c_{TX} \cdot \left|\Omega_{TX}^{(c)}\right|, b_{RX} \cdot \left|\Omega_{RX}^{(c)}\right| \right\},$$

$$d_{\mathsf{img}} + d_{\mathsf{comm}} \leq \frac{2T}{\lambda} \cdot b_{RX} \cdot \left| \Omega_{RX}^{(i)} \cup \Omega_{RX}^{(c)} \right|.$$

Proof: See Appendix A. ∎

We now describe the proposed decode-and-image scheme.

B. Decode-and-Image: Joint Processing at BS

The proposed decode-and-image scheme operates in two phases consisting of uplink pilot and data transmission.

1) Phase 1: Phase 1 spans the first $T_1 \leq T$ slots. In Phase 1, the uplink user transmits time-orthogonal pilot symbols $\mathbf{X}_{T_1}^{(c)}$ that the BS uses to form an initial estimate of the scene. To that end, since the channel $\mathbf{H}_{\mathsf{known}}^{(c)}$ and pilots $\mathbf{X}_{T_1}^{(c)}$ are known, the BS subtracts out $\mathbf{H}_{\mathsf{known}}^{(c)} \cdot \mathbf{X}_{T_1}^{(c)}$ to obtain

$$\mathbf{y}_{T_1}^{(i)} = \mathsf{vec}\left(\mathbf{Y}_{T_1} - \mathbf{H}_{\mathsf{known}}^{(c)} \cdot \mathbf{X}_{T_1}^{(c)}\right) = \mathbf{H}_{\mathsf{vec}}^{(i)} \cdot \mathbf{f} + \mathbf{n}_{T_1},$$

$$\mathbf{H}_{\mathsf{vec}}^{(i)} = \left(\begin{bmatrix}\mathbf{X}_{T_1}^{(i)}\\ \mathbf{X}_{T_1}^{(c)}\end{bmatrix}^{\top} \otimes \mathbf{I}_{K_{RX}}\right) \cdot \left(\begin{bmatrix}\mathbf{P}_{TX}^{(i)} * \mathbf{P}_{RX}^{(i)}\\ \mathbf{P}_{TX}^{(c\cap i)} * \mathbf{P}_{RX}^{(c\cap i)}\end{bmatrix}\right).$$

Note that the matrix $\mathbf{H}_{\mathsf{vec}}^{(i)}$ is known to the BS receiver as per Assumption 5. Thus, the BS recovers $\mathbf{f}$ via

$$\hat{\mathbf{f}}_{(1)} = \left(\mathbf{H}_{\mathsf{vec}}^{(i)}\right)^{\dagger} \cdot \mathbf{y}_{T_1}^{(i)},$$

where the subscript $(\cdot)_{(1)}$ denotes Phase 1.

2) Phase 2: Phase 2 spans the remaining $(T - T_1)$ slots. The goal of the BS in this phase is to (i) decode the uplink data, with the reflectivity estimate $\hat{\mathbf{f}}_{(1)}$ as side-information, and (ii) image the scene, with the decoded data as side-information. To that end, the BS and uplink user perform beamforming on the basis of the available prior knowledge:

1) One possibility is to decode the uplink symbols by beamforming according to the SVD of $\mathbf{H}_{\mathsf{known}}^{(c)} = \mathbf{U}_{\mathsf{known}}^{(c)} \cdot \mathbf{\Sigma}_{\mathsf{known}}^{(c)} \cdot \left(\mathbf{V}_{\mathsf{known}}^{(c)}\right)^{H}$ alone,

$$\left(\mathbf{U}_{\mathsf{known}}^{(c)}\right)^{H} \cdot \mathbf{Y}_{(T-T_1)} = \mathbf{\Sigma}_{\mathsf{known}}^{(c)} \cdot \left(\mathbf{V}_{\mathsf{known}}^{(c)}\right)^{H} \cdot \mathbf{X}_{(T-T_1)}^{(c)},$$

where the noise term has been suppressed for clarity.

2) The second possibility is to decode the uplink symbols by beamforming according to the SVD of $\mathbf{H}^{(c)} = \mathbf{U}^{(c)} \cdot \mathbf{\Sigma}^{(c)} \cdot \left(\mathbf{V}^{(c)}\right)^{H}$, estimated using $\hat{\mathbf{f}}_{(1)}$ from Phase 1,

$$\left(\mathbf{U}^{(c)}\right)^{H} \cdot \mathbf{Y}_{(T-T_1)} = \mathbf{\Sigma}^{(c)} \cdot \left(\mathbf{V}^{(c)}\right)^{H} \cdot \mathbf{X}_{(T-T_1)}^{(c)},$$

where the noise term has been suppressed for clarity.

The BS subsequently recovers $\mathbf{f}$ via

$$\hat{\mathbf{f}} = \left(\mathbf{H}_{\mathsf{vec}}^{(i)}\right)^{\dagger} \cdot \mathsf{vec}\left(\mathbf{Y}_T - \mathbf{H}_{\mathsf{known}}^{(c)} \cdot \mathbf{X}_T^{(c)}\right),$$

where $\mathbf{H}_{\mathsf{vec}}^{(i)}$ is defined similar to Phase 1, except over all T slots instead of the first T_1.

We now present an inner bound on the DoF region.

C. Inner Bound $\mathcal{D}_{\mathsf{in}}$ on DoF Region

To derive an inner bound $\mathcal{D}_{\mathsf{in}} \subseteq \mathcal{D}$ on the DoF region, we characterize the set of *achievable* imaging and communication DoF pairs, defined as per Definition 7, for different decode-and-image parameter values, i.e., Phase 1 duration T_1, illumination symbols $\mathbf{X}_T^{(i)}$, and choice of beamforming matrices. The following theorem characterizes the inner bound $\mathcal{D}_{\mathsf{in}}$.

Theorem 2: An inner bound $\mathcal{D}_{\mathsf{in}}$ on the DoF region $\mathcal{D}$ is the convex closure of the set comprising the following DoF pairs,

$$\begin{aligned}
\mathsf{P}'_0 &= (d_{\mathsf{img}}, d_{\mathsf{comm}}) = (0,0)\,,\\
\mathsf{P}'_1 &= (d_{\mathsf{img}}, d_{\mathsf{comm}}) = (\Delta_{\mathsf{img}}, 0)\,,\\
\mathsf{P}'_2 &= (d_{\mathsf{img}}, d_{\mathsf{comm}}) = (\Delta_{\mathsf{img}}, \Delta'_{\mathsf{comm}})\,,\\
\mathsf{P}'_3 &= (d_{\mathsf{img}}, d_{\mathsf{comm}}) = \left(\Delta'_{\mathsf{img}}, \Delta_{\mathsf{comm}}\right),\\
\mathsf{P}'_4 &= (d_{\mathsf{img}}, d_{\mathsf{comm}}) = (0, \Delta_{\mathsf{comm}})\,,
\end{aligned}$$

where Δ_{img} is the maximum imaging DoF as per Theorem 1,

$$\Delta_{\mathsf{img}} = \frac{2}{\lambda} \cdot \min\Big\{b_{RX} \cdot \left|\Omega_{RX}^{(i)}\right| \cdot \chi, b_{TX} \cdot \left|\Omega_{TX}^{(i)}\right| + c_{TX} \cdot \left|\Omega_{TX}^{(c\cap i)}\right| + b_{RX} \cdot \left|\Omega_{RX}^{(i)}\right|\Big\},$$

and Δ'_{img} is smaller than Δ_{img}, and equals

$$\Delta'_{\mathsf{img}} = \frac{2}{\lambda} \cdot \min\Big\{b_{RX} \cdot \left|\Omega_{RX}^{(i)}\right| \cdot \chi, b_{TX} \cdot \left|\Omega_{TX}^{(i\setminus c)}\right| + c_{TX} \cdot \left|\Omega_{TX}^{(c\cap i)}\right| + b_{RX} \cdot \left|\Omega_{RX}^{(i)}\right|\Big\},$$

where $\Omega_{TX}^{(i\setminus c)}$ is the angular interval corresponding to the portion of the imaging scene illuminated by the BS alone and

$$\chi = \lim_{\substack{K_{TX}^{(i)} \to \infty \\ K_{TX}^{(c)} \to \infty}} \mathsf{rank}\left(\begin{bmatrix}\mathbf{X}_T^{(i)}\\ \mathbf{X}_T^{(c)}\end{bmatrix}\right).$$

The maximum possible communication DoF, Δ_{comm}, is

$$\begin{aligned}
\Delta_{\mathsf{comm}} &= \frac{2}{\lambda} \cdot \max\left\{(T - T_1) \cdot \alpha, T \cdot \beta\right\},\\
T_1 &= \left\lceil \frac{\left|\Omega_{RX}^{(i)} \cap \Omega_{RX}^{(c)}\right|}{\left|\Omega_{RX}^{(i)}\right|} + \frac{c_{TX} \cdot \left|\Omega_{TX}^{(c\cap i)}\right|}{b_{RX} \cdot \left|\Omega_{RX}^{(i)}\right|} \right\rceil,\\
\alpha &= \min\left\{c_{TX} \cdot \left|\Omega_{TX}^{(c)}\right|, b_{RX} \cdot \left|\Omega_{RX}^{(c)}\right|\right\},\\
\beta &= \min\left\{c_{TX} \cdot \left|\Omega_{TX}^{(c)} \setminus \Omega_{TX}^{(c\cap i)}\right|, b_{RX} \cdot \left|\Omega_{RX}^{(c)} \setminus \Omega_{RX}^{(i)}\right|\right\}.
\end{aligned}$$

The term Δ'_{comm} is identical to Δ_{comm}, except with

$$T_1 = \left\lceil 1 + \frac{c_{TX} \cdot \left|\Omega_{TX}^{(c\cap i)}\right| + b_{TX} \cdot \left|\Omega_{TX}^{(i)}\right|}{b_{RX} \cdot \left|\Omega_{RX}^{(i)}\right|} \right\rceil.$$

Proof: See Appendix B. ∎

We next evaluate the gap between the inner and outer bounds, and show that it is vanishingly small in the regime $T \to \infty$. Thus, decode-and-image is asymptotically optimal.

D. Asymptotic Optimality of Decode-and-Image

Consider the limit of large channel coherence intervals, $T \to \infty$. In this regime, we show that decode-and-image is asymptotically optimal, i.e., the gap between the inner bound $\mathcal{D}_{\mathsf{in}}$ from Theorem 2 and the DoF region $\mathcal{D}$ is vanishingly small compared to the measure of $\mathcal{D}$.

Theorem 3: Decode-and-image is asymptotically optimal under the limit of large channel coherence intervals, i.e.,

$$\lim_{T\to\infty} \frac{|\mathcal{D} - \mathcal{D}_{\mathsf{in}}|}{|\mathcal{D}|} = 0,$$

where $|\mathcal{A}|$ denotes the Lebesgue measure of a set $\mathcal{A}$,

Proof: See Appendix C. ∎

In the next section, we provide a system-level illustration of our main results for the signal space model in Figure 2.

V. System-Level Illustration of Main Results

To illustrate our main results from Section IV, we consider two simple cases. In the first case in Section V-A, we characterize the impact of the *spatial overlap* between the scene and uplink channel clusters on the DoF region. We show that increasing the spatial overlap between the scene and uplink channel clusters results in better imaging performance at the cost of a smaller decoding rate. Furthermore, in the special case with zero spatial overlap between the scene and uplink channel clusters, we show that both decode-and-image and zero-forcing are optimal, i.e., achieve the outer bound $\mathcal{D}_{\mathsf{out}}$.

In the second case in Section V-B, we study the impact of the *aperture sizes* at the BS and uplink user on the DoF region. In the special case where the scene is only illuminated by the uplink signals, we show that decode-and-image enables opportunistic imaging for a small reduction in the uplink rate.

In both cases, we also show that decode-and-image outperforms schemes that do not jointly process the imaging and communication signals. To that end, we compare the inner bound from Theorem 2 with the achievable DoF region for time division multiple access (TDMA) and the zero-forcing successive interference cancellation (SIC) scheme from [25]. TDMA corresponds to time-sharing between BS illumination and uplink communication, whereas the zero-forcing scheme from [25] corresponds to spatially isolating the imaging and communication signals. Unlike decode-and-image, neither of the considered schemes utilize the uplink signals for imaging.

A. Case 1: Effect of Spatial Overlap

Consider a symmetric version of Figure 2 with identical volumes of radii b at all nodes, i.e., $b_{TX} = b_{RX} = c_{TX} = b$. By constraining all nodes to be symmetric, we aim to isolate the impact of the channel angular intervals from our results from Section IV. To reduce the number of variables in the DoF expressions, we further constrain all transmit and receive angular intervals to have equal measure,

$$\left|\Omega_{TX}^{(i)}\right| = \left|\Omega_{RX}^{(i)}\right| = |\Omega_{\mathsf{img}}|\,,$$
$$\left|\Omega_{TX}^{(c)}\right| = \left|\Omega_{RX}^{(c)}\right| = |\Omega_{\mathsf{comm}}|\,.$$

Hence, we shall quantify the effect of the angular domain *overlap*, $|\Omega_{\mathsf{img}} \cap \Omega_{\mathsf{comm}}|$, between the scene and uplink channel clusters on the DoF region. Without loss of generality, for the purpose of this example we shall assume $|\Omega_{\mathsf{img}}| \leq |\Omega_{\mathsf{comm}}|$.

We focus our attention on the regime where the space-time DoF at the BS for imaging exceeds the number of parallel channels for imaging. As per Theorem 1, the same requires

$$\lim_{\substack{K_{TX}^{(i)}\to\infty \\ K_{TX}^{(c)}\to\infty}} \mathsf{rank}\left(\begin{bmatrix}\mathbf{X}_T^{(i)} \\ \mathbf{X}_T^{(c)}\end{bmatrix}\right) \geq \frac{2b\cdot|\Omega_{\mathsf{img}}| + b\cdot|\Omega_{\mathsf{img}}\cap\Omega_{\mathsf{comm}}|}{b\cdot|\Omega_{\mathsf{img}}|},$$

or equivalently, coherence intervals of length $T \geq 3$, assuming the matrices $\mathbf{X}_T^{(i)}$ and $\mathbf{X}_T^{(c)}$ are time-orthogonal.

In this regime, the outer bound in Theorem 1 simplifies to

$$d_{\mathsf{img}} \leq \frac{2}{\lambda}\cdot\left(2b\cdot|\Omega_{\mathsf{img}}| + b\cdot|\Omega_{\mathsf{img}}\cap\Omega_{\mathsf{comm}}|\right),$$
$$d_{\mathsf{comm}} \leq \frac{2T}{\lambda}\cdot b\cdot|\Omega_{\mathsf{comm}}|\,,$$
$$d_{\mathsf{img}} + d_{\mathsf{comm}} \leq \frac{2T}{\lambda}\cdot b\cdot|\Omega_{\mathsf{img}}\cup\Omega_{\mathsf{comm}}|\,.$$

Moreover, the terms in the inner bound from Theorem 2 are

$$\Delta_{\mathsf{img}} = \frac{2b}{\lambda}\cdot\left(2\cdot|\Omega_{\mathsf{img}}| + |\Omega_{\mathsf{img}}\cap\Omega_{\mathsf{comm}}|\right),$$
$$\Delta'_{\mathsf{img}} = \frac{2b}{\lambda}\cdot\left(2\cdot|\Omega_{\mathsf{img}}|\right),$$
$$\Delta_{\mathsf{comm}} = \frac{2b}{\lambda}\cdot\max\left\{(T-2)\cdot|\Omega_{\mathsf{comm}}|\,, T\cdot|\Omega_{\mathsf{comm}}\setminus\Omega_{\mathsf{img}}|\right\},$$
$$\Delta'_{\mathsf{comm}} = \frac{2b}{\lambda}\cdot\max\left\{(T-3)\cdot|\Omega_{\mathsf{comm}}|\,, T\cdot|\Omega_{\mathsf{comm}}\setminus\Omega_{\mathsf{img}}|\right\}.$$

To interpret the above bounds, we consider three representative overlap regimes:

1) the *zero overlap* regime with disjoint imaging and communication angular spreads, i.e., $\Omega_{\mathsf{img}} \cap \Omega_{\mathsf{comm}} = \emptyset$,
2) the *partial overlap* regime with non-disjoint angular spreads, i.e., $\Omega_i \setminus \Omega_j \subset \Omega_i,\ \forall i \neq j \in \{\mathsf{img}, \mathsf{comm}\}$,
3) the *full overlap* regime with fully overlapping angular spreads, i.e., $\Omega_{\mathsf{img}} \setminus \Omega_{\mathsf{comm}} = \emptyset$.

We plot the outer bound in the three regimes in Figure 3(a).

1) Zero Overlap Regime: In the zero overlap regime, no uplink communication signals bounce off the imaging scene. Thus, simple zero-forcing suffices to spatially isolate the imaging and communication signals for scene reconstruction and decoding respectively, and the outer bound is *rectangular*.

Moreover, since $\Omega_{\mathsf{img}} \cap \Omega_{\mathsf{comm}} = \emptyset$, both the inner and outer bounds match in the zero overlap regime, i.e., $\Delta_{\mathsf{comm}} = \Delta'_{\mathsf{comm}}$ and $\Delta_{\mathsf{img}} = \Delta'_{\mathsf{img}}$. Thus, decode-and-image is optimal in this regime. Furthermore, zero overlap is sufficient for a rectangular DoF region $\mathcal{D}$ for all coherence intervals $T \geq 2$.

Remark 1: The DoF region $\mathcal{D}$ is rectangular if $T \geq 2$ and $|\Omega_{\mathsf{img}} \cap \Omega_{\mathsf{comm}}| = 0$.

However, since $\Omega_{\mathsf{img}} \cap \Omega_{\mathsf{comm}} = \emptyset$, the maximum imaging DoF only corresponds to BS illumination and reception, i.e., $\Delta_{\mathsf{img}} = \Delta'_{\mathsf{img}} = \frac{2b}{\lambda}\cdot(2\cdot|\Omega_{\mathsf{img}}|)$. Thus, while zero overlap results in a rectangular DoF region, there is no imaging benefit of uplink illumination in this case.

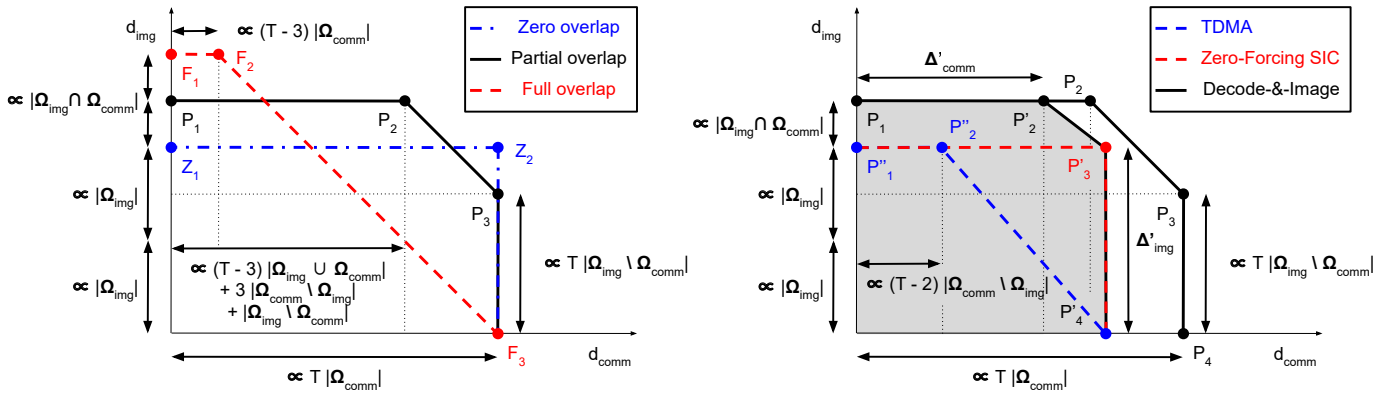

Fig. 3: Illustration of bounds for Case 1 from Section V-A. (a) Outer bound $\mathcal{D}_{\text{out}}$ in three overlap regimes. The imaging DoF increases and uplink rate decreases with increasing overlap $|\Omega_{\text{img}} \cap \Omega_{\text{comm}}|$. (b) Inner bounds (shaded) for decode-and-image, TDMA and zero-forcing SIC, and outer bound (non-shaded) in partial overlap regime. Decode-and-image outperforms both TDMA and zero-forcing SIC.

2) Partial Overlap Regime: When the imaging and communication angular spreads are not disjoint, both the inner and outer bounds exhibit an imaging DoF gain proportional to the overlap $|\Omega_{\text{img}} \cap \Omega_{\text{comm}}|$ compared to BS-only illumination. However, the non-zero overlap also results in a smaller communication DoF compared to the maximum possible. Thus, the imaging benefit of uplink illumination comes at the cost of a smaller uplink rate.

3) Full Overlap Regime: In the full overlap regime, the maximum imaging DoF and reduction in uplink rate are both largest since all uplink signals bounce off the scene. Furthermore, the inner bound matches exactly with the outer bound for all DoF pairs satisfying $d_{\text{comm}} \leq \Delta_{\text{comm}}$, i.e., $\mathcal{D}_{\text{in}} = \mathcal{D}_{\text{out}} \cap \{d_{\text{comm}} \leq \Delta_{\text{comm}}\}$.

4) Comparison with Isolation-based Schemes: Finally, we compare our inner bound with TDMA and zero-forcing SIC. TDMA corresponds to time-sharing between the BS transmitter and uplink user. Let $\gamma \in [0,1]$ denote the fraction of the coherence interval allocated to the imaging flow. Via similar analysis as Theorem 2, the inner bound for TDMA is

$$d_{\text{img}} \leq \frac{2b}{\lambda} \cdot \min\left\{ |\Omega_{\text{img}}| \cdot \lim_{K_{TX}^{(i)} \to \infty} \text{rank}\left(\mathbf{X}_{\gamma T}^{(i)}\right), 2 \cdot |\Omega_{\text{img}}| \right\},$$

$$d_{\text{comm}} \leq \frac{2\,(1-\gamma)\,T}{\lambda} \cdot b \cdot |\Omega_{\text{comm}} \setminus \Omega_{\text{img}}|\,,$$

whereas the equivalent region for zero-forcing SIC is

$$d_{\text{img}} \leq \frac{4b}{\lambda} \cdot |\Omega_{\text{img}}|\,,$$

$$d_{\text{comm}} \leq \frac{2\,(1-\gamma)\,T}{\lambda} \cdot b \cdot |\Omega_{\text{comm}} \setminus \Omega_{\text{img}}|\,.$$

Both regions above are subsets of the rectangular region $\left\{d_{\text{img}} \leq \frac{4b}{\lambda} \cdot |\Omega_{\text{img}}|\right\}$, which in turn is a subset of $\mathcal{D}_{\text{in}}$ since $\Delta'_{\text{img}} = \frac{4b}{\lambda} \cdot |\Omega_{\text{img}}|$ in Theorem 2. Hence, decode-and-image always outperforms TDMA and zero-forcing SIC for all overlap values, $\mathcal{D}_{\text{in,TDMA}} \subset \mathcal{D}_{\text{in,SIC}} \subset \mathcal{D}_{\text{in}}$.

In Figure 3(b), we compare $\mathcal{D}_{\text{in,TDMA}}$, $\mathcal{D}_{\text{in,SIC}}$, $\mathcal{D}_{\text{in}}$, and $\mathcal{D}_{\text{out}}$ in the partial overlap regime. Clearly, joint processing results in significant performance gains that are not achievable using schemes that perform imaging and communication in isolation.

B. Case 2: Effect of Aperture Sizes

Consider the full overlap regime from Section V-A, where (a) the imaging and communication signals impinge onto the BS over the same angles, $\Omega_{RX}^{(i)} = \Omega_{RX}^{(c)}$, and (b) all uplink signals illuminate the entire scene, i.e., $\Omega_{TX}^{(c \cap i)} = \Omega_{TX}^{(c)}$ and $\Omega_{TX}^{(i \setminus c)} = \emptyset$. To reduce the number of variables in the DoF expressions, we further constrain all angular spreads to have equal measure, $\left|\Omega_{TX}^{(i)}\right| = \left|\Omega_{RX}^{(i)}\right| = \left|\Omega_{TX}^{(c)}\right| = \left|\Omega_{RX}^{(c)}\right| = |\Omega|$. These angular spread constraints allow us to isolate the impact of the aperture sizes, b_{TX}, b_{RX} and c_{TX} on the DoF region.

As before, we consider the regime where the space-time DoF at the BS for imaging exceeds the number of parallel channels for imaging. As per Theorem 1, the same requires

$$\lim_{\substack{K_{TX}^{(i)} \to \infty \\ K_{TX}^{(c)} \to \infty}} \text{rank}\left(\begin{bmatrix} \mathbf{X}_T^{(i)} \\ \mathbf{X}_T^{(c)} \end{bmatrix}\right) \geq \frac{b_{TX} + b_{RX} + c_{TX}}{b_{RX}},$$

i.e., coherence intervals of length $T \geq \left\lceil \frac{b_{TX}+b_{RX}+c_{TX}}{b_{RX}} \right\rceil$, assuming the matrices $\mathbf{X}_T^{(i)}$ and $\mathbf{X}_T^{(c)}$ are time-orthogonal.

In this regime, the outer bound in Theorem 1 simplifies to

$$d_{\text{img}} \leq \frac{2}{\lambda} \cdot (b_{TX} + b_{RX} + c_{TX}) \cdot |\Omega|\,,$$

$$d_{\text{comm}} \leq \frac{2T}{\lambda} \cdot \min\{c_{TX}, b_{RX}\} \cdot |\Omega|\,,$$

$$d_{\text{img}} + d_{\text{comm}} \leq \frac{2T}{\lambda} \cdot b_{RX} \cdot |\Omega|\,.$$

It is easy to see that the bound is rectangular under the following condition.

Remark 2: The outer bound $\mathcal{D}_{\text{out}}$ is rectangular iff

$$T \geq \frac{b_{TX} + b_{RX} + c_{TX}}{[b_{RX} - c_{TX}]^+},$$

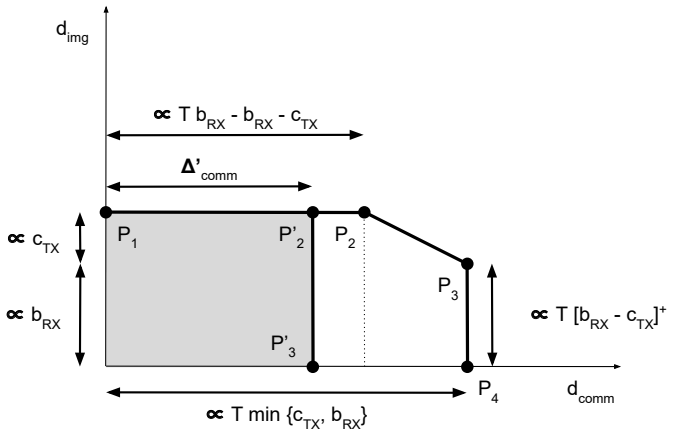

Fig. 4: Comparison of inner (shaded) and outer (non-shaded) bounds in partial overlap regime for Case 2 from Section V-B when $b_{TX} = 0$. The inner bound is rectangular in this case.

where $[x]^+$ denotes the positive part of x.

Note that the bound above diverges to ∞ when the uplink user has a larger spherical volume compared to the BS, i.e., $c_{TX} \geq b_{RX}$. Hence, Remark 2 is an *impossibility* result; when $c_{TX} \geq b_{RX}$, the outer bound $\mathcal{D}_{\mathsf{out}}$ can never be rectangular.

We now consider the inner bound from Theorem 2. The terms in the inner bound are

$$\Delta_{\mathsf{img}} = \frac{2}{\lambda} \cdot (b_{TX} + b_{RX} + c_{TX}) \cdot |\Omega|\,,$$
$$\Delta'_{\mathsf{img}} = \frac{2}{\lambda} \cdot (b_{RX} + c_{TX}) \cdot |\Omega|\,,$$
$$\Delta_{\mathsf{comm}} = \frac{2}{\lambda} \cdot (T-2) \cdot \min\{c_{TX}, b_{RX}\} \cdot |\Omega|\,,$$
$$\Delta'_{\mathsf{comm}} = \frac{2}{\lambda} \cdot (T-T_1) \cdot \min\{c_{TX}, b_{RX}\} \cdot |\Omega|\,,$$
$$T_1 = \left\lceil \frac{b_{TX} + b_{RX} + c_{TX}}{b_{RX}} \right\rceil \geq 2.$$

Note that when $c_{TX} = b_{RX}$, the two bounds match the bounds for Case 1 in the full overlap regime. Furthermore, we have the following condition on the inner bound.

Remark 3: The inner bound $\mathcal{D}_{\mathsf{in}}$ is rectangular iff $b_{TX} = 0$.

The $b_{TX} = 0$ case above is practically interesting since it corresponds to no BS illumination, i.e., the scene is only illuminated by the uplink signals. Imaging in this case is *opportunistic*, in the sense that the BS aims to passively image the scene being illuminated by the a-priori unknown uplink signals. As per Remark 3, decode-and-image achieves a *rectangular* subset of the outer bound, i.e., allows for imaging and communication to co-exist with no trade-off, for only a small reduction in the communication DoF (2 slots) compared to the outer bound. We illustrate the outer and inner bounds for the $b_{TX} = 0$ case in Figure 4.

Finally, we compare our inner bound against TDMA and zero-forcing SIC. Unlike Section V-A, in this example neither scheme can achieve a communication DoF greater than zero since the set of interference-free angles is empty, $\Omega^{(c)}_{RX} \setminus \Omega^{(i)}_{RX} = \emptyset$. Hence, decode-and-image trivially outperforms both TDMA and zero-forcing SIC in this case.

VI. Concluding Remarks

In this paper, we quantified the fundamental performance trade-offs between imaging and uplink communication supported simultaneously by a dual-function base station. To that end, we proposed a unified signal space analysis framework based on the degrees of freedom metric and a dual-function joint processing scheme, decode-and-image. Our analysis and proposed scheme highlighted the benefits of exploiting the uplink signals for imaging, at the cost of increased cooperation between the base station and uplink user. Moreover, our proposed scheme was shown to outperform traditional schemes that enable dual-function operation via spatial or temporal isolation of imaging and communication signals.

A limitation of our present analysis and proposed scheme is the requirement of prior knowledge about the communication channel and path delay matrices at the base station. In future work, we aim to extend our results to the "blind" setting with no such prior knowledge. Similar to prior results on non-coherent multi-user communication [35], we expect a smaller DoF region in this regime. Furthermore, we shall extend our analysis to the downlink system configuration as well as hybrid configurations with both uplink and downlink users.

Appendix A
Proof of Theorem 1

Throughout this proof, we use the signal space notation introduced in Section III and illustrated in Figure 2.

We begin by deriving the maximum imaging DoF. We assume genie-aided knowledge of the uplink symbols $\mathbf{X}^{(c)}_T$ at the BS. Hence, the BS performs imaging by subtracting out the known communication signals $\mathbf{H}^{(c)}_{\mathsf{known}} \cdot \mathbf{X}^{(c)}_T$ from the receive measurements. The resulting measurements are $\mathbf{H}^{(i)}_{\mathsf{vec}} \cdot \mathbf{f} + \mathbf{n}_T$,

$$\mathbf{H}^{(i)}_{\mathsf{vec}} = \left(\begin{bmatrix} \mathbf{X}^{(i)}_T \\ \mathbf{X}^{(c)}_T \end{bmatrix}^{\top} \otimes \mathbf{I}_{K_{RX}} \right) \cdot \left(\begin{bmatrix} \mathbf{P}^{(i)}_{TX} * \mathbf{P}^{(i)}_{RX} \\ \mathbf{P}^{(c\cap i)}_{TX} * \mathbf{P}^{(c\cap i)}_{RX} \end{bmatrix} \right).$$

Via (3), we have $d_{\mathsf{img}} \leq \lim_{\substack{\left(K^{(i)}_{TX}, K^{(c)}_{TX}\right) \to \infty \\ (K_{RX}, M) \to \infty}} \mathsf{rank}\left(\mathbf{H}^{(i)}_{\mathsf{vec}}\right)$,

$$\mathsf{rank}\left(\mathbf{H}^{(i)}_{\mathsf{vec}}\right) = \min\left\{ K_{RX} \cdot \mathsf{rank}\left(\begin{bmatrix} \mathbf{X}^{(i)}_T \\ \mathbf{X}^{(c)}_T \end{bmatrix} \right), \mathsf{rank}\left(\begin{bmatrix} \mathbf{P}^{(i)}_{TX} * \mathbf{P}^{(i)}_{RX} \\ \mathbf{P}^{(c\cap i)}_{TX} * \mathbf{P}^{(c\cap i)}_{RX} \end{bmatrix} \right) \right\}.$$

On applying Lemma 1, well-known properties of the Khatri-Rao product and the main results of [38], we obtain

$$d_{\mathsf{img}} \leq \lim_{\substack{\left(K^{(i)}_{TX}, K^{(c)}_{TX}\right) \to \infty \\ (K_{RX}, M) \to \infty}} \min\left\{ \frac{2b_{RX}}{\lambda} \cdot \left|\Omega^{(i)}_{RX}\right| \cdot \mathsf{rank}\left(\begin{bmatrix} \mathbf{X}^{(i)}_T \\ \mathbf{X}^{(c)}_T \end{bmatrix} \right), \right.$$
$$\left. \frac{2b_{TX}}{\lambda} \cdot \left|\Omega^{(i)}_{TX}\right| + \frac{2c_{TX}}{\lambda} \cdot \left|\Omega^{(c\cap i)}_{TX}\right| + \frac{2b_{RX}}{\lambda} \cdot \left|\Omega^{(i)}_{RX}\right| \right\},$$

which yields the desired imaging DoF upper bound. Compared to BS-only illumination, genie-aided knowledge of uplink symbols at the BS results in an imaging DoF gain proportional to $\left|\Omega^{(c\cap i)}_{TX}\right|$ due to additional uplink user illumination.

Next, let us consider communication. We assume genie-aided knowledge of the reflectivities $\mathbf{f}$ at the BS receiver. Hence, the BS simply decodes the communication message

using its knowledge of the channel $\mathbf{H}^{(c)}$, which achieves the communication DoF bound from Lemma 1.

Finally, the sum of the imaging and communication DoFs is bounded by the total BS resource d_{BS} from Definition 6. The outer bound $\mathcal{D}_{\mathsf{out}}$ is given by the convex closure of DoF pairs $(d_{\mathsf{img}}, d_{\mathsf{comm}})$ that satisfy the three DoF inequalities.

Appendix B
Proof of Theorem 2

We shall only show achievability of the corner points P'_1 to P'_4, since all other points in $\mathcal{D}_{\mathsf{in}}$ are achievable either trivially (point P'_0) or via time-sharing (interior of $\mathcal{D}_{\mathsf{in}}$).

Point P'_1 corresponds to imaging-only. Thus, we choose $T_1 = T$, i.e., the uplink user transmits pilots for the whole coherence interval. The achievable communication DoF is zero. Applying the imaging algorithm from Phase 1 over the entire coherence interval yields $d_{\mathsf{img}} = \Delta_{\mathsf{img}}$, where Δ_{img} is as defined in the theorem statement. Hence, point P'_1 is achieved.

Point P'_4 corresponds to communication-only. Thus, we choose $\mathbf{X}_T^{(i)} = \mathbf{0}$, i.e., the BS transmitter remains silent for the whole coherence interval. There are two possibilities here:

1) Use the first beamformer in Phase 2 with $T_1 = 0$,
2) Use the second beamformer for an appropriate $T_1 > 0$.

For the first choice, the achievable communication DoF is

$$d_{\mathsf{comm}} = \tfrac{2T}{\lambda} \cdot \min\left\{ c_{TX} \cdot \left|\Omega_{TX}^{(c)} \setminus \Omega_{TX}^{(c\cap i)}\right|, b_{RX} \cdot \left|\Omega_{RX}^{(c)} \setminus \Omega_{RX}^{(i)}\right| \right\},$$

on applying Lemma 1 to the corresponding measurements.

For the second choice, we first find the optimal value of T_1 to maximize the imaging DoF corresponding to the Phase 1 estimate $\hat{\mathbf{f}}_{(1)}$. To that end, since $\mathbf{X}_T^{(i)} = \mathbf{0}$, we have $\mathbf{H}_{\mathsf{vec}}^{(i)} = \left(\left(\mathbf{X}_{T_1}^{(c)}\right)^{\top} \otimes \mathbf{I}_{K_{RX}}\right) \cdot \left(\mathbf{P}_{TX}^{(c\cap i)} * \mathbf{P}_{RX}^{(c\cap i)}\right)$. Hence, to achieve the imaging DoF upper bound from (3), $\mathbf{X}_{T_1}^{(c)}$ must satisfy

$$\lim_{K_{TX}^{(c)} \to \infty} \mathsf{rank}\left(\mathbf{X}_{T_1}^{(c)}\right) \geq \frac{\left|\Omega_{RX}^{(i)} \cap \Omega_{RX}^{(c)}\right|}{\left|\Omega_{RX}^{(i)}\right|} + \frac{c_{TX} \cdot \left|\Omega_{TX}^{(c\cap i)}\right|}{b_{RX} \cdot \left|\Omega_{RX}^{(i)}\right|}.$$

Since the pilots $\mathbf{X}_{T_1}^{(c)}$ are time-orthogonal, we choose

$$T_1 = \left\lceil \frac{\left|\Omega_{RX}^{(i)} \cap \Omega_{RX}^{(c)}\right|}{\left|\Omega_{RX}^{(i)}\right|} + \frac{c_{TX} \cdot \left|\Omega_{TX}^{(c\cap i)}\right|}{b_{RX} \cdot \left|\Omega_{RX}^{(i)}\right|} \right\rceil,$$

as the smallest value required to satisfy the above condition.

Via Lemma 1, the communication DoF is thus $d_{\mathsf{comm}} = \frac{2(T-T_1)}{\lambda} \cdot \min\left\{ c_{TX} \cdot \left|\Omega_{TX}^{(c)}\right|, b_{RX} \cdot \left|\Omega_{RX}^{(c)}\right| \right\}$. Point P'_4 corresponds to the maximum among the two DoF values.

We now consider points P'_2 and P'_3, both of which correspond to joint processing at the BS. To achieve P'_3, the BS transmitter only beamforms along $\Omega_{TX}^{(i\setminus c)}$, the angular interval corresponding to the portion of the imaging scene illuminated by the BS alone. Thus, the imaging and communication signals are spatially isolated, and the exact same decoding scheme from the achievability of point P'_4 can be used. The achievable communication DoF is Δ_{comm}. Once the uplink message is decoded, the imaging DoF $d_{\mathsf{img}} = \lim_{\substack{\left(K_{TX}^{(i)}, K_{TX}^{(c)}\right) \to \infty \\ (K_{RX}, M) \to \infty}} \mathsf{rank}\left(\mathbf{H}_{\mathsf{vec}}^{(i)}\right) = \Delta'_{\mathsf{img}}$ is subsequently achievable, where Δ'_{img} is as defined in the theorem statement, for $\mathbf{H}_{\mathsf{vec}}^{(i)}$ defined appropriately considering the BS transmitter only beamforms along $\Omega_{TX}^{(i\setminus c)}$. Note that Δ'_{img} is smaller than the maximum possible DoF Δ_{img} due to the smaller angular interval illuminated by the BS.

Finally, to achieve P'_2, we again consider the two choices from the achievability of point P'_4 for decoding the uplink message. For the first choice, the communication DoF remains unchanged. For the second choice, T_1 must satisfy

$$T_1 = \left\lceil 1 + \frac{c_{TX} \cdot \left|\Omega_{TX}^{(c\cap i)}\right| + b_{TX} \cdot \left|\Omega_{TX}^{(i)}\right|}{b_{RX} \cdot \left|\Omega_{RX}^{(i)}\right|} \right\rceil.$$

Note that the above T_1 value is larger than that for point P'_4. Thus, the maximum of the resulting DoFs, Δ'_{comm}, is smaller than the maximum possible DoF Δ_{comm}. Finally, the subsequent imaging algorithm achieves the maximum possible DoF Δ_{img}, similar to point P'_1. Hence, point P'_2 is achieved.

The inner bound $\mathcal{D}_{\mathsf{in}}$ is given by the convex closure of the points P'_0 through P'_4.

Appendix C
Proof of Theorem 3

We begin by deriving the measures of the inner and outer bounds from Theorems 1 and 2. Via basic geometry, the measure of the inner bound is given by

$$|\mathcal{D}_{\mathsf{in}}| = \Delta_{\mathsf{comm}} \cdot \Delta_{\mathsf{img}} - \frac{\left(\Delta_{\mathsf{comm}} - \Delta'_{\mathsf{comm}}\right) \cdot \left(\Delta_{\mathsf{img}} - \Delta'_{\mathsf{img}}\right)}{2},$$

where all symbols are defined as in Theorem 2. Note that Δ_{img} and $\left(\Delta_{\mathsf{img}} - \Delta'_{\mathsf{img}}\right)$ are constants. Furthermore, under the limit $T \to \infty$, the term $\left(\Delta_{\mathsf{comm}} - \Delta'_{\mathsf{comm}}\right)$ is also a constant,

$$\lim_{T \to \infty} \left(\Delta_{\mathsf{comm}} - \Delta'_{\mathsf{comm}}\right) = \frac{1}{\lambda} \cdot \left(T'_1 - T_1\right) \cdot \alpha = \mathcal{O}\left(1\right),$$

where T_1 and T'_1 are the values of T_1 from Theorem 2 corresponding to Δ_{comm} and Δ'_{comm} respectively. The term α is as defined in Theorem 2. Hence, the measure of the inner bound scales as $|\mathcal{D}_{\mathsf{in}}| = \mathcal{O}\left(T\right)$ due to the term Δ_{comm}.

Via a similar calculation, the outer bound has measure

$$|\mathcal{D}_{\mathsf{out}}| = \tfrac{2T}{\lambda} \cdot \alpha \cdot \Delta_{\mathsf{img}} - \frac{\left(\left[\Delta_{\mathsf{img}} - \frac{2T}{\lambda} \cdot b_{RX} \cdot \left|\Omega_{RX}^{(i)} \cup \Omega_{RX}^{(c)}\right| + \frac{2T}{\lambda} \cdot \alpha\right]^{+}\right)^2}{2}.$$

Note that $|\mathcal{D}_{\mathsf{out}}|$ above may be upper and lower bounded as

$$\frac{2T}{\lambda} \cdot \alpha \cdot \Delta_{\mathsf{img}} - \frac{\left(\Delta_{\mathsf{img}}\right)^2}{2} \leq |\mathcal{D}_{\mathsf{out}}| \leq \frac{2T}{\lambda} \cdot \alpha.$$

Since the bounds on $|\mathcal{D}_{\mathsf{out}}|$ scale proportional to T, we have $|\mathcal{D}_{\mathsf{out}}| = \mathcal{O}\left(T\right)$ as well. Since the DoF region $\mathcal{D}$ is sandwiched between the inner and outer bounds, $\mathcal{D}_{\mathsf{in}} \subseteq \mathcal{D} \subseteq \mathcal{D}_{\mathsf{out}}$, we must thus have $|\mathcal{D}| = \mathcal{O}\left(T\right)$.

Now, consider the gap between the inner and outer bounds,

$$|\mathcal{D}_{\mathsf{out}} - \mathcal{D}_{\mathsf{in}}| = \left(\frac{2T}{\lambda} \cdot \alpha - \Delta_{\mathsf{comm}}\right) \cdot \Delta_{\mathsf{img}} + \mathcal{O}\left(1\right),$$

where all constants have been absorbed into the $\mathcal{O}(1)$ term. Via the definition of Δ_{comm} from Theorem 2, we obtain

$$\left(\frac{2T}{\lambda}\cdot\alpha-\Delta_{\mathsf{comm}}\right)=\frac{2}{\lambda}\cdot\min\left\{T_1\cdot\alpha,T\cdot(\alpha-\beta)\right\}.$$

Under the limit $T\to\infty$, the right hand side is constant,

$$\lim_{T\to\infty}\left(\frac{2T}{\lambda}\cdot\alpha-\Delta_{\mathsf{comm}}\right)=\frac{2T_1}{\lambda}\cdot\alpha=\mathcal{O}(1).$$

Hence, the gap between the two bounds is also a constant, i.e., $|\mathcal{D}_{\mathsf{out}}-\mathcal{D}_{\mathsf{in}}|=\mathcal{O}(1)$. Since $\mathcal{D}-\mathcal{D}_{\mathsf{in}}\subseteq\mathcal{D}_{\mathsf{out}}-\mathcal{D}_{\mathsf{in}}$, we must thus have $|\mathcal{D}-\mathcal{D}_{\mathsf{in}}|=\mathcal{O}(1)$, which vanishes compared to the measure of $\mathcal{D}$ as $T\to\infty$. Hence, decode-and-image is asymptotically optimal.

REFERENCES

[1] N. Mehrotra and A. Sabharwal, "Simultaneous Imaging & Uplink Communication: A Degrees of Freedom Perspective," in *2021 55th Asilomar Conference on Signals, Systems, and Computers*, 2021.

[2] F. Adib and D. Katabi, "See through Walls with WiFi!" in *Proceedings of the ACM SIGCOMM 2013 Conference on SIGCOMM*, ser. SIGCOMM '13, 2013, p. 75–86.

[3] D. Huang, R. Nandakumar, and S. Gollakota, "Feasibility and Limits of Wi-Fi Imaging," in *Proceedings of the 12th ACM Conference on Embedded Network Sensor Systems*, ser. SenSys '14, 2014, p. 266–279.

[4] P. M. Holl and F. Reinhard, "Holography of Wi-fi Radiation," *Phys. Rev. Lett.*, vol. 118, p. 183901, May 2017.

[5] S. Vakalis, L. Gong, and J. A. Nanzer, "Imaging With WiFi," *IEEE Access*, vol. 7, pp. 28 616–28 624, 2019.

[6] D. Sheen, D. McMakin, and T. Hall, "Three-dimensional millimeter-wave imaging for concealed weapon detection," *IEEE Transactions on Microwave Theory and Techniques*, vol. 49, no. 9, pp. 1581–1592, 2001.

[7] Y. Zhu, Y. Zhu, B. Y. Zhao, and H. Zheng, "Reusing 60GHz Radios for Mobile Radar Imaging," in *Proceedings of the 21st Annual International Conference on Mobile Computing and Networking*, ser. MobiCom '15. New York, NY, USA: Association for Computing Machinery, 2015, p. 103–116. [Online]. Available: https://doi.org/10.1145/2789168.2790112

[8] A. Pedross-Engel, D. Arnitz, J. N. Gollub, O. Yurduseven, K. P. Trofatter, M. F. Imani, T. Sleasman, M. Boyarsky, X. Fu, D. L. Marks, D. R. Smith, and M. S. Reynolds, "Orthogonal Coded Active Illumination for Millimeter Wave, Massive-MIMO Computational Imaging With Metasurface Antennas," *IEEE Transactions on Computational Imaging*, vol. 4, no. 2, pp. 184–193, 2018.

[9] J. Guan, A. Paidimarri, A. Valdes-Garcia, and B. Sadhu, "3-D Imaging Using Millimeter-Wave 5G Signal Reflections," *IEEE Transactions on Microwave Theory and Techniques*, vol. 69, no. 6, pp. 2936–2948, 2021.

[10] A. Diebold, M. Imani, and D. Smith, "Phaseless Radar Coincidence Imaging with a MIMO SAR Platform," *Remote Sensing*, vol. 11, no. 5, p. 533, Mar 2019.

[11] R. Heckel, "Super-Resolution Radar Imaging via Convex Optimization," *Compressed Sensing in Radar Signal Processing*, p. 193, 2019.

[12] B. Yonel, I.-Y. Son, and B. Yazici, "Exact Multistatic Interferometric Imaging via Generalized Wirtinger Flow," *IEEE Transactions on Computational Imaging*, vol. 6, pp. 711–726, 2020.

[13] A. Akhtar, B. Yonel, and B. Yazici, "Passive Multistatic Radar Imaging with Prior Information," in *2021 IEEE Radar Conference (RadarConf21)*, 2021, pp. 1–6.

[14] T. M. Cover and J. A. Thomas, *Elements of Information Theory*, 2nd ed. USA: Wiley-Interscience, 2006.

[15] O. M. Bucci and G. Franceschetti, "On the Degrees of Freedom of Scattered Fields," *IEEE Transactions on Antennas and Propagation*, vol. 37, no. 7, pp. 918–926, July 1989.

[16] A. S. Y. Poon, R. W. Brodersen, and D. N. C. Tse, "Degrees of Freedom in Multiple-Antenna Channels: A Signal Space Approach," *IEEE Transactions on Information Theory*, vol. 51, no. 2, pp. 523–536, Feb 2005.

[17] M. Franceschetti, M. D. Migliore, and P. Minero, "The capacity of wireless networks: Information-theoretic and physical limits," *IEEE Transactions on Information Theory*, vol. 55, no. 8, pp. 3413–3424, 2009.

[18] E. Everett and A. Sabharwal, "Spatial degrees-of-freedom in large-array full-duplex: the impact of backscattering," *EURASIP Journal on Wireless Communications and Networking*, vol. 2016, no. 1, pp. 1–23, 2016.

[19] M. Franceschetti, *Wave Theory of Information*. Cambridge University Press, Nov 2017.

[20] S. Vedantam, W. Zhang, U. Mitra, and A. Sabharwal, "Joint Channel Estimation and Data Transmission: Achievable Rates," in *2007 IEEE Information Theory Workshop*. IEEE, 2007, pp. 499–504.

[21] M. Kobayashi, G. Caire, and G. Kramer, "Joint State Sensing and Communication: Optimal Tradeoff for a Memoryless Case," in *2018 IEEE International Symposium on Information Theory (ISIT)*. IEEE, 2018, pp. 111–115.

[22] M. Kobayashi, H. Hamad, G. Kramer, and G. Caire, "Joint State Sensing and Communication over Memoryless Multiple Access Channels," in *2019 IEEE International Symposium on Information Theory (ISIT)*, 2019, pp. 270–274.

[23] M. Bica, K.-W. Huang, U. Mitra, and V. Koivunen, "Opportunistic Radar Waveform Design in Joint Radar and Cellular Communication Systems," in *2015 IEEE Global Communications Conference (GLOBECOM)*, 2015, pp. 1–7.

[24] M. Bica, K.-W. Huang, V. Koivunen, and U. Mitra, "Mutual information based radar waveform design for joint radar and cellular communication systems," in *2016 IEEE International Conference on Acoustics, Speech and Signal Processing (ICASSP)*, 2016, pp. 3671–3675.

[25] Y. Rong, A. R. Chiriyath, and D. W. Bliss, "Multiple-Antenna Multiple-Access Joint Radar and Communications Systems Performance Bounds," in *2017 51st Asilomar Conference on Signals, Systems, and Computers*. IEEE, 2017, pp. 1296–1300.

[26] Y. Gao, H. Li, and B. Himed, "Joint Transmit and Receive Beamforming for Hybrid Active–Passive Radar," *IEEE Signal Processing Letters*, vol. 24, no. 6, pp. 779–783, 2017.

[27] F. Wang and H. Li, "Joint waveform and receiver design for co-channel hybrid active-passive sensing with timing uncertainty," *IEEE Transactions on Signal Processing*, vol. 68, pp. 466–477, 2020.

[28] C. Li, N. Raymondi, B. Xia, and A. Sabharwal, "Outer Bounds for a Joint Communicating Radar (Comm-Radar): The Uplink Case," *IEEE Transactions on Communications*, pp. 1–1, 2021.

[29] R. Piestun and D. A. B. Miller, "Electromagnetic degrees of freedom of an optical system," *Journal of the Optical Society of America A*, vol. 17, no. 5, p. 892, May 2000.

[30] F. M. Dickey, L. A. Romero, J. M. DeLaurentis, and A. W. Doerry, "Super-resolution, degrees of freedom and synthetic aperture radar," *IEE Proceedings - Radar, Sonar and Navigation*, vol. 150, no. 6, pp. 419–429, Dec 2003.

[31] B. Mamandipoor, A. Arbabian, and U. Madhow, "Geometry-constrained Degrees of Freedom Analysis for Imaging Systems: Monostatic and Multistatic," *arXiv: Information Theory*, Nov 2017. [Online]. Available: http://arxiv.org/abs/1711.03585

[32] M. Franceschetti, "On Landau's Eigenvalue Theorem and Information Cut-Sets," *IEEE Transactions on Information Theory*, vol. 61, no. 9, pp. 5042–5051, Sep. 2015.

[33] A. Pinkus, *n-widths in Approximation Theory*. Springer-Verlag, 1985.

[34] Y. Wu, S. Shamai Shitz, and S. Verdú, "Information Dimension and the Degrees of Freedom of the Interference Channel," *IEEE Transactions on Information Theory*, vol. 61, no. 1, pp. 256–279, 2015.

[35] C. Huang, S. A. Jafar, S. Shamai, and S. Vishwanath, "On Degrees of Freedom Region of MIMO Networks Without Channel State Information at Transmitters," *IEEE Transactions on Information Theory*, vol. 58, no. 2, pp. 849–857, 2012.

[36] D. Tse and P. Viswanath, *Fundamentals of Wireless Communication*. Cambridge University Press, 2005.

[37] O. Yurduseven, J. N. Gollub, K. P. Trofatter, D. L. Marks, A. Rose, and D. R. Smith, "Software Calibration of a Frequency-Diverse, Multistatic, Computational Imaging System," *IEEE Access*, vol. 4, pp. 2488–2497, 2016.

[38] G. Marsaglia and G. P. H. Styan, "Equalities and Inequalities for Ranks of Matrices," *Linear and Multilinear Algebra*, vol. 2, no. 3, pp. 269–292, 1974. [Online]. Available: https://doi.org/10.1080/03081087408817070

Nishant Mehrotra received the B.Tech. degree (with honors) in Electronics and Electrical Communication Engineering from the Indian Institute of Technology, Kharagpur, India in 2018 and the M.S. degree in Electrical and Computer Engineering from Rice University, Houston, TX, USA in 2020. He is currently pursuing the Ph.D. degree in Electrical and Computer Engineering at Rice University, Houston, TX, USA. His research interests include information theory, joint sensing-communication, and wireless systems.

Ashutosh Sabharwal received the B.Tech. degree from IIT Delhi, New Delhi, India, in 1993, and the M.S. and Ph.D. degrees from The Ohio State University, Columbus, OH, USA, in 1995 and 1999, respectively. He is currently the Department Chair and Ernest D. Butcher Professor at the Department of Electrical and Computer Engineering, Rice University, Houston, TX, USA. His research interests are in wireless theory, design, and large-scale deployed testbeds. He is the founder of the WARP project (warp.rice.edu), an open-source project which is now in use at more than 125 research groups worldwide and has been used by more than 500 research articles. He is currently leading several NSF-funded center-scale projects, notably Rice RENEW (renew-wireless.org), to develop an open-source software-defined wireless network platform. He received the 2017 IEEE Jack Neubauer Memorial Award, 2018 IEEE Advances in Communications Award, 2019 ACM MobiCom Community Contribution Award, and the 2019 and 2021 ACM Test-of-time Awards. He is a Fellow of IEEE and the National Academy of Inventors.